



ELSEVIER

Contents lists available at [SciVerse ScienceDirect](http://www.sciencedirect.com)

Nuclear Instruments and Methods in Physics Research A

journal homepage: www.elsevier.com/locate/nima

Unexploded Ordnance identification—A gamma-ray spectral analysis method for Carbon, Nitrogen and Oxygen signals following tagged neutron interrogation

S. Mitra^{a,*}, I. Dioszegi^b^a Environmental Sciences Department, Brookhaven National Laboratory, Bell Avenue, Upton, NY 11973, USA^b Nonproliferation and National Security Department, Brookhaven National Laboratory, Upton, NY 11973, USA

ARTICLE INFO

Article history:

Received 10 February 2012

Received in revised form

17 July 2012

Accepted 24 July 2012

Available online 2 August 2012

Keywords:

UXO identification

Associated particle technique

Monte Carlo simulation

Spectral analysis

ABSTRACT

A novel gamma-ray spectral analysis method has been demonstrated to optimally extract the signals of the signature elements of explosives, carbon (C), nitrogen (N) and oxygen (O) from 57–155 mm projectiles following tagged neutron interrogation with 14 MeV neutrons. The method was implemented on Monte Carlo simulated, synthetic spectra of Unexploded Ordnance (UXO) that contained high explosive fillers (Composition B, TNT or Explosive D) within steel casings of appropriate thicknesses. The analysis technique defined three broad regions-of-interest (ROI) between 4–7.5 MeV of a spectrum and from a system of three equations for the three unknowns namely C, N and O, the maximum counts from each of these elements were extracted. Unlike conventional spectral analysis techniques, the present method included the Compton continuum under a spectrum. For a neutron output of $\sim 2 \times 10^7 \text{ ns}^{-1}$ and using four 12.7 cm diameter \times 12.7 cm NaI(Tl) detectors, the C/N and C/O gamma-ray counts ratios of the explosive fillers were vastly different from that of an inert substance like sand. Conversion of the counts ratios to elemental ratios could further discriminate the different types of explosive fillers. The interrogation time was kept at ten minutes for each projectile.

© 2012 Elsevier B.V. All rights reserved.

1. Introduction

Identification of the fillers of Unexploded Ordnance (UXO) as high explosive (HE) or inert is an expensive task to the armed forces of many countries for their efficient remediation. The inert substances used are often physically similar to the HE, such as density, to provide the same ballistic behavior but mostly contain no nitrogen. Some of the commonly used inert fillers are sand, concrete, or wax [1,2]. Cost effective and non-destructive technologies requiring short inspection times with low false alarm rates are required. In a real-world situation, this must be accomplished in a cluttered environment that also contains non-hazardous items.

Carbon (C), Nitrogen (N) and Oxygen (O) are signature elements for explosives detection particularly because of their unique C/O and C/N elemental ratios which allow their discrimination from benign substances [3]. Fast neutron induced production of characteristic gamma-rays from C, N and O and their detection is a potentially sensitive non-destructive technique and reviews on the topic have been published [4,5]. However, neutrons also produce gamma-rays from all surrounding matter

and the signal/noise ratios are poor. In a field situation, it is particularly severe for those UXOs lying on soil or is partially buried in it. Signals from the O of soil will be a major interference while a cascading de-excitation of Si in soil from the 6.27 MeV state to the 1.78 MeV state following the $^{28}\text{Si}(n,n'\gamma)^{28}\text{Si}$ reaction, produces 4.49 MeV gamma-rays that will interfere with the C analysis at 4.43 MeV. This interference has been determined to be as high as 40% and 19% of the net C signal from experiments in a sand pit containing 2.5% and 10% C by weight respectively [6]. In addition, the inelastic scattering cross-sections of fast neutrons with N for producing the major lines at 2.31, 4.46 and 5.1 MeV is low (about a factor of three lower) than the production cross-sections of the major lines of 4.43 and 6.13 MeV from C and O respectively [7], resulting in a very weak signal intensity which is not observable above the high background from surrounding material. This precludes the use of conventional micro-second pulsed 14 MeV neutron interrogation methods for observing the signals due to fast neutron induced inelastic scattering reactions with N. The problems with measuring N using its gamma-ray emissions via fast neutron scattering has been further described in a recent critical review on photon and neutron interrogation techniques for explosives detection [8].

Over the past few years, the associated particle technique (APT) is increasingly being used for explosives detection [9–11].

* Corresponding author. Tel.: +1 631 344 6377.

E-mail address: sudeepmitra@hotmail.com (S. Mitra).

With knowledge of the neutron direction and time-of-flight information, the technique assures high signal/noise ratios by accepting signals mainly from the suspect object. As a result, it also became possible to simultaneously observe the fast neutron induced signals from C, N and O. Using simple targets like graphite and water, we had earlier demonstrated through proof-of-concept studies the efficacy of the APT for obtaining gamma-ray signals from an object-of-interest with high signal-noise ratio and without interference from signals of near-by clutter [12]. Although signal/noise ratios are high, inter element interferences exist among C, N and O. High resolution detectors like HPGe cannot resolve these interferences particularly in the C signal because C is also one of the end products of neutron interactions with O via the $^{16}\text{O}(n,n'\alpha)^{12}\text{C}$. In recent reports that implement the APT, the neutron induced gamma-ray spectrum of an unknown material is first fitted with a linear combination of the individual elemental signatures from a library of gamma-ray signatures to unfold the spectra of C, N and O. This is followed by decision-making steps which involves using either 'fuzzy logic' procedures [13] or converting the C, N and O counts ratios to elemental ratios using an extensive set of conversion factors based on Monte Carlo numerical simulations [14,15]. The latter reports note that the conversion factors rely upon knowledge of the neutron energy spectrum at the location of the inspected object and the attenuation of gamma-rays between their production point and the detectors. More importantly, Compton scattering in the cargo materials induces a low energy component that introduces systematic spectrum unfolding uncertainties when using a pure element database acquired with bare samples. In view of these observations, it is realized that a robust gamma spectroscopy technique would be the key for the detection of these elements and the reliable identification of explosives.

The present study deals with a simple manipulation of spectra offered by the APT and are a modification of a spectral analysis scheme developed earlier for extracting C, N and O signals for the in vivo determination of fat, protein and water in live sheep [16]. While, N and O were previously determined from the 5–7 MeV region of the spectrum, the spectral analysis method being reported here de-convolves the inter-elemental interferences among C, N and O and extracts the total signal of gamma-rays for N and O from the 4–7.5 MeV region of the spectrum. This modification now includes the signals due to the 4.43 MeV lines from N and O. C was determined as usual from its 4.43 MeV line. There are no signals from C above 4.43 MeV.

The procedure uses only the spectral response of the detector system for the 4–7.5 MeV region of the gamma-ray spectrum produced due to inelastic scattering reactions of fast neutrons with C, N and O. It does not require a library of pure elemental spectra, or information on the neutron energy or gamma-ray attenuation in the interrogated object. Using the method, signal counts from C, N and O were determined from Monte Carlo simulated spectra of UXOs (with appropriate steel case thicknesses and containing high explosive (HE) fillers like Composition B, TNT or Explosive D) ranging from 57 mm mortars to 155 mm projectiles following 14 MeV neutron interrogation with the APT. The counts ratios of the explosives were converted to elemental ratios using factors related to their known elemental ratios. The counts ratios and their conversion have been utilized to differentiate the HE fillers from an inert substance like sand and to differentiate the HE fillers from each other.

2. Methods

Synthetic spectra were obtained using MCNPX v27e Monte Carlo simulations [17] and the most recent ENDF/B-VII data

library. Using such a simulation, it was recently reported [18,19] that a good qualitative agreement was obtained between the synthetic and experimental gamma-ray spectra of C, N and O. The neutron induced gamma-ray flux and its time distribution at the detector surface was determined using the F5 point detector tally. The tally was then processed using the MODAR package [20]. This package is able to read in the MCNPX output file, extract two dimensional energy-time tally data, and place energy and time windows to select subsets of the data as is usually done with experimental data. Additionally, MODAR allows smearing the time and energy spectra independently with a normal distribution and a gamma detector response function respectively to reproduce effects of the experimental time and energy resolutions. The detector response functions generated in the energy range 0.1 MeV–8.5 MeV and the Gaussian energy broadening of the F8 tally that takes into account the measured energy resolution of the detector was adapted from the work of Carasco [20]. Photons were injected under a normal incidence on the small face ($12.7\text{ cm} \times 12.7\text{ cm}$) of a $12.7\text{ cm} \times 12.7\text{ cm} \times 25.4\text{ cm}$ NaI(Tl) detector. The energy resolutions for this detector were reported to be 7.39 and 4.62% for Cs (0.662 MeV) and C (4.43 MeV) respectively [21] and compared closely with our 12.5 cm diameter by 12.7 cm NaI(Tl) detector: 7.4 and 3.8% for Cs and C respectively.

2.1. Geometry

Two geometries were set-up to: (1) Benchmark the simulation and (2) Interrogate UXOs of different sizes.

- (1) Benchmark the simulation—The geometry was identical to the proof-of-concept studies [12]. The tagged neutron beam was modeled using a 45 degree conical source. This was based on the geometry of the neutron generator (NG) that we used for the proof-of-concept studies; the cone being defined by the NG's alpha detector dimension and its distance from the tritium target. 14 MeV neutron source particles were tracked towards a graphite target (cube of dimension 15.2 cm) situated at a distance of 27 cm from the neutron source with a corresponding detector-sample distances of 55 cm. The 45 degree angle between the neutron beam and the sample to detector axis was included in the geometry. The set-up is shown in Fig. 1.

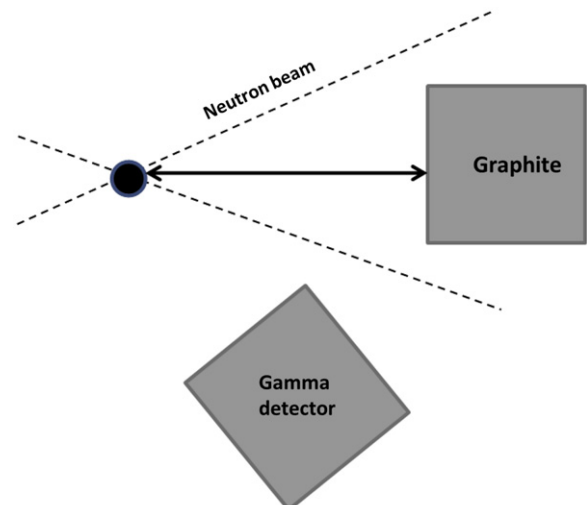


Fig. 1. Geometry for benchmarking the simulation.

(2) Interrogate UXOs of different sizes—For all runs the base of the neutron cone had a diameter equal to the outer diameter of the UXO at its mid-line along the long-axis. The neutron source distance to the long axis thus varied from 5.7–15.5 cm for the 57–155 mm projectiles. The NaI(Tl) detector was positioned on top of the UXO at a distance of 30 cm from its mid-line. To model the soil effects, the UXO was made to rest on a $50 \times 50 \times 50$ cm cube of sand (composition: SiO_2). This area and volume of soil was considered to be adequate because the largest beam diameter at the sample was 15.5 cm. The schematics of the geometry are shown in Fig. 2.

2.2. Description of the UXOs

The UXOs modeled in this study were 57–155 mm projectiles. Their shell thicknesses and HE fillers are summarized in Table 1 and the chemical composition data of the fillers are presented in Table 2.

2.3. Spectral analysis algorithm

The prompt gamma-rays of interest, namely the full energy peaks from fast-neutron inelastic scattering with C, N and O are

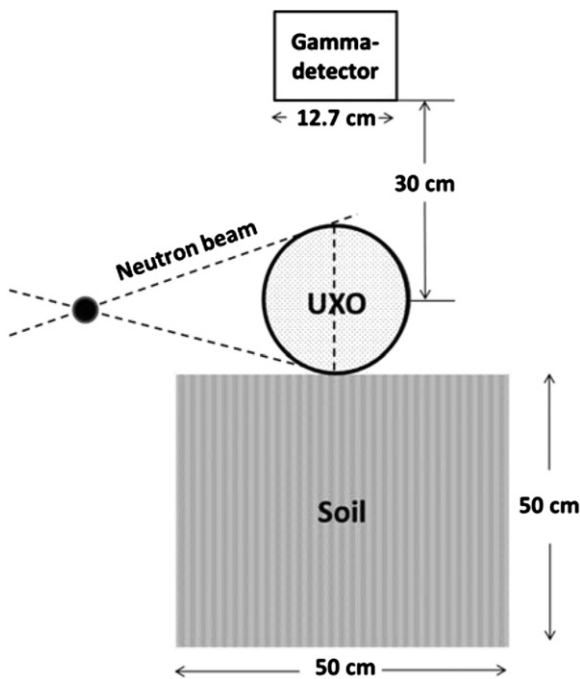


Fig. 2. Geometry for modeling the UXO interrogation.

Table 1

Data showing the type of high explosive fillers and shell thicknesses of the UXOs in the 57–155 mm range.

UXO size, mm	Ordnance Data Sheet D2US[22]	Shell thickness, mm	Filler	Amount of charge, gms
57	000033	6.7 ^a	Explosive D	NA ^b
60	000171	6.7	Composition B	190
75	000204	9.8	TNT	700
81	000280	9.0 ^a	Composition B	1,000
105	000337	13.0 ^a	Composition B	2,300
155	000550	14.0	Composition B	6,900

^a The shell thicknesses were not documented in the data sheets and the values are approximate.

^b Data not available. MCNPX uses weight % and density and the amount of charge is not a constraint.

Table 2

Chemical composition of the high explosive fillers.

Filler	Weight, %				Density, g/cm ³
	C	H	N	O	
Composition B ^a	24.5	2.5	30.1	42.8	1.65
TNT	37.0	2.2	18.5	42.3	1.65
Explosive D (Ammonium Picrate)	29.3	2.4	22.8	45.5	1.72

^a 60% RDX and 40% TNT mixture by weight.

C(4.43 MeV), N(7.03, 5.1, 5.03 and 4.46 MeV) and O (7.12, 6.92, 6.13 and 4.43 MeV). N has a full energy peak at 2.31 MeV which could be used for determining the element away from the C and O interferences at 4.43 MeV but will suffer from interference by Al emission at 2.21 MeV (a common structural material). Consequently, signals are extracted from the 4.0–7.5 MeV regions where the only elemental interferences are among C, N and O. The additional advantage with this scheme is that higher energy signals in the 4.0–7.5 MeV regions are more penetrating than the 2.31 MeV gamma-rays and will therefore be more effectively detected when emanating from an UXO with various steel case thicknesses.

The following strategies were adopted to extract counts from a spectrum:

- (1) The Compton continuum is included unlike in the conventional method of spectral analysis where the Compton events under a peak are rejected as background noise.
- (2) If an element contributed gamma-rays to two different regions-of-interest (ROI) then the respective contributions were determined by measuring the ratio of the intensities in the two regions. This is particularly important for determining the lower energy Compton continuum produced due to higher energy gamma-rays interacting in the detector. The contribution of the counts to the different ROIs and their ratios are related to the spectral response of the detector being used, and in particular, will (a) depend on the size of the detector being employed and (b) be independent of the amount of element. These coefficients are accurately determined experimentally.
- (3) Since there were three mutually interfering contributions to the spectrum from C, N and O, a system of three equations were designed for the three unknown components. To maximize the signal-to-noise ratio and improve the standard deviation for low count rates expected in coincidence spectroscopy, three large ROIs were selected. Further, the end-points of the regions were located in a valley of the spectrum to minimize bin-to-bin fluctuations while calibrating for energy. ROI₁ was set between 5.34–6.41 MeV which mainly included the prominent O full energy and its escape peak due to the 6.13 MeV de-excitation. This region was nested within a second larger region, ROI₂, which was set from 4.84–7.44 MeV and included all the possible signals from N and O between 5–7 MeV. The third region, ROI₃, was from 4.24–4.71 MeV and included C, N and O signals. There is no contribution to ROI₁ and ROI₂ from C.

A system of three equations for the three unknowns, namely C, N and O, was obtained as follows:

$$ROI_1 = aX_O + bX_N \quad (1)$$

$$ROI_2 = X_O + X_N \quad (2)$$

$$ROI_3 = cX_O + dX_N + X_C \quad (3)$$

where X_O and X_N are the total number of counts in the spectrum from oxygen and nitrogen respectively in ROI₁ and ROI₂, a the ratio of oxygen counts in ROI₁/ROI₂ to give aX_O as the counts due to oxygen in ROI₁, b the ratio of nitrogen counts in ROI₁/ROI₂ to give bX_N as the counts due to nitrogen in ROI₁, c the ratio of oxygen counts in ROI₃/ROI₂ to give cX_O as the O counts in ROI₃ from the 4.43 MeV yield produced from the $^{16}\text{O}(n, n'\alpha)^{12}\text{C}$ reaction, d the ratio of nitrogen counts in ROI₃/ROI₂ to give dX_N as the N counts from the 4.46 MeV yield in ROI₃ and X_C is the number of counts due to carbon from its 4.43 MeV de-excitation in ROI₃. Solving Eqs. (1–3)

$$X_N = (aROI_2 - ROI_1)/(a-b) \quad (4)$$

$$X_O = ROI_2 - X_N \quad (5)$$

$$X_C = ROI_3 - cX_O - dX_N \quad (6)$$

The total counts of N and O in the 4–7.5 MeV regions can be obtained as

$$X_{N\text{total}} = X_{N(4.84-7.44 \text{ MeV})} + dX_{N(4.24-4.71 \text{ MeV})} \quad (7)$$

$$X_{O\text{total}} = X_{O(4.84-7.44 \text{ MeV})} + cX_{O(4.24-4.71 \text{ MeV})} \quad (8)$$

The C/N and C/O elemental ratios can be related to the counts ratios as follows:

$$C/N = k_1(X_C/X_{N\text{total}}) \quad (9)$$

$$C/O = k_2(X_C/X_{O\text{total}}) \quad (10)$$

The conversion factors k_1 and k_2 are determined from targets with known C/N and C/O elemental ratios and are related to the ratio of the differential neutron interaction cross-sections and gamma-ray attenuations.

Using an appropriate geometry, the coefficients, a and c , were obtained from the MCNPX/MODAR synthetic spectrum of liquid oxygen (density, 1.14 g/cc) while coefficients b and d , were obtained from N in the form of liquid nitrogen (density, 0.81 g/cc). Fig. 3 depicts the ROIs that were used for determining the coefficients while Table 3 shows the values of the coefficients that were determined for extracting C, N and O counts. Errors reported for

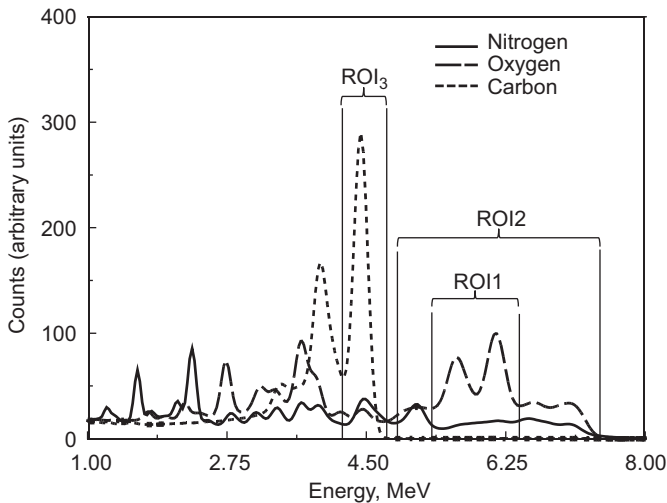


Fig. 3. Synthetic gamma-ray spectra of C, N and O showing the different Regions-Of-Interest (ROI) for determining the interference coefficients and extracting the elemental counts. ROI₁ was set at 5.34–6.41 MeV, ROI₂ was 4.84–7.44 MeV and ROI₃ was 4.24–4.71 MeV.

Table 3

Coefficients, a , b , c and d for the different regions-of-interest (ROI).

Element	Oxygen "a" ROI ₁ /ROI ₂	Nitrogen "b" ROI ₁ /ROI ₂	Oxygen "c" ROI ₃ /ROI ₂	Nitrogen "d" ROI ₃ /ROI ₂
Carbon	–	–	–	–
Nitrogen	–	0.394 ± 0.002	–	0.334 ± 0.002
Oxygen	0.610 ± 0.002	–	0.104 ± 0.001	–

the coefficients, a , b , c , and d , the C, N and O counts and the constants k_1 and k_2 are a result of the error propagations due to the counting statistics ($\sqrt{\text{counts}}$) of ROI₁, ROI₂ and ROI₃.

3. Results and discussion

3.1. Benchmarking the simulation

Since MCNPX computes the probability distributions of events for a given number of source particles (10 million source neutrons in the present simulations) and normalizes the result per source neutron, the simulation results are scaled to match the experimental data in terms of the run time, and neutron emission. The scaling factor required ($\sim 10^5$) for matching with the experimental spectrum of the graphite block, indicated that the tagged beam represented about 1% of the total isotropic neutron emission of $\sim 10^7 \text{ ns}^{-1}$; the neutron emission rate was determined by using the Cu foil activation method to provide a base line data for the neutron generator output [12].

Fig. 4a shows the comparison of the smeared time spectrum with that obtained experimentally for the graphite. Smearing with a 2 ns standard deviation time resolution function could fit the experimental time window that was used for determining the time-correlated gamma-ray spectrum. Since the modeling did not take into account the time correlated gamma-ray production from the neutron generator material (iron) or its immediate vicinity (shown as dashed area), or from those neutrons scattering from the graphite target and interacting (inelastic scattering) with the detector material (peak labeled as neutron scattering), the calculation shows only a single time peak, which is generated from the gamma-rays coming from the graphite sample. The features to the left and right of the main peak noticed in the experimental time peak were thus absent. Also, since the random background from uncorrelated events was not modeled, for a proper comparison, this background was estimated from the region shown in Fig. 4a and added to the simulated time spectrum. Fig. 4b shows a comparison of the corresponding time correlated gamma-ray spectra of the simulation and experiment after the simulated spectrum was smeared and scaled for experimental run time and neutron flux. A linear background was determined under the experimental spectrum in the region 2.5–5.0 MeV and added to the synthetic spectrum. The experimental and synthetic gamma-ray spectral shapes are in good agreement. The shapes are different at energies below 2 MeV because a threshold of 1.5 MeV was set for the experimental runs.

3.2. Interrogation of UXOs in the 57–155 mm range

The gamma-ray counts obtained per source neutron for a single NaI(Tl) detector were scaled for a ten minute interrogation time, an isotropic neutron output of $2 \times 10^7 \text{ ns}^{-1}$ (twice the output used for the benchmarking studies) and four 12.5 cm diameter \times 12.5 cm detectors to generate the synthetic spectrum for each projectile. The explosive fillers and the shell thicknesses of the projectiles are summarized in Table 1. Fig. 5 shows the

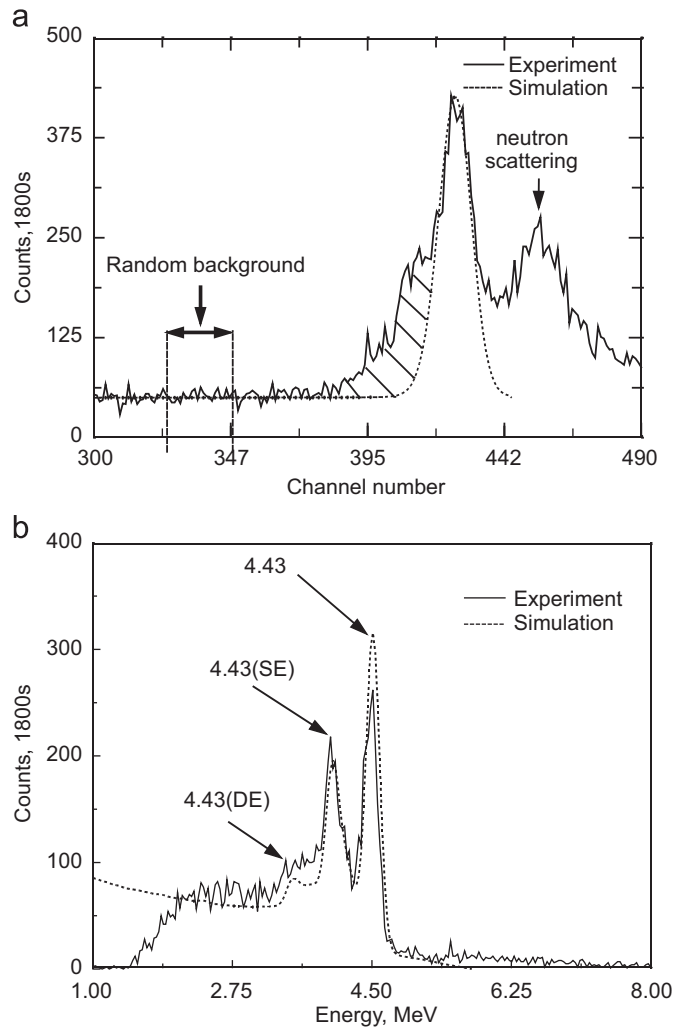


Fig. 4. (a) Experimental and simulated time-of-flight spectra for the graphite sample at a distance of 27 cm from the neutron source. The diagonally dashed area corresponds to gamma-rays from the neutron generator walls and nearby objects, (b) the time correlated experimental and simulated synthetic spectrum showing the main, single (SE) and double escape (DE) peaks.

synthetic spectra of all the projectiles (57–155 mm) situated in air. The C, N and O counts obtained with the analytic scheme is summarized in Table 4. Data are presented for the UXO placed either in air or on the soil surface. Values generated by the algorithm for soil (SiO_2) with no UXO in the beam are also presented. The statistical errors of the C, N and O counts reported here are propagations from the statistical variability of ROI₁, ROI₂ and ROI₃ which included the random background. To estimate this background and its effect if any, on the statistical variability, data from the proof-of-concept studies [12] was used; the background from uncorrelated events was determined by recording the gamma-ray spectrum with a time window from the random background region of the time spectrum (see Fig. 4a). The background is estimated to be $\sim 3\%$ of the total counts of ROI₁, ROI₂ or ROI₃ for a 155 mm projectile and $\sim 6\%$ for the 57 mm projectile. Thus, the errors on the net background-subtracted counts for any ROI, as a result of the error propagation due to the random background, would change only by a few counts and will not affect the errors being reported. The C counts generated for soil are due to the 4.49 MeV gamma-rays of a de-excitation from the 6.27 MeV state to the 1.78 MeV state of Si as mentioned earlier. The N counts generated in soil are obviously an artifact because of the N coefficient, “a” operating on the ROI₂. Further, it has been

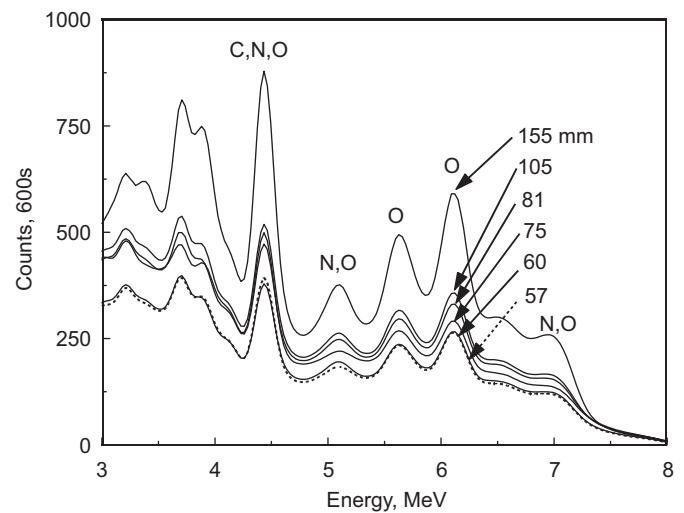


Fig. 5. Synthetic spectra of the projectiles situated in air. Values per source neutron for a single NaI(Tl) detector were scaled for a ten minute interrogation time, an isotropic neutron output of $2 \times 10^7 \text{ ns}^{-1}$ and four 12.5 cm diameter \times 12.5 cm detectors.

Table 4

The C, N and O gamma-ray counts from UXOs for a ten minute interrogation time using four 12.5 cm \times 12.5 cm NaI(Tl) detectors and a neutron output of $2 \times 10^7 \text{ ns}^{-1}$. Values for soil (sand) are obtained without the UXO in the neutron beam.

UXO size, mm	Surface	Counts/600 s		
		C	N	O
57	Air	2047 \pm 203	6195 \pm 575	10394 \pm 561
	Soil(4ns cut)	1703 \pm 207	5528 \pm 589	11748 \pm 575
60	Air	1846 \pm 204	6910 \pm 581	10266 \pm 567
	Soil(4 ns cut)	1525 \pm 207	6003 \pm 589	11390 \pm 575
75	Air	2686 \pm 222	8213 \pm 626	11542 \pm 611
	Soil(4.5 ns cut)	2263 \pm 225	7417 \pm 640	12746 \pm 624
81	Air	2311 \pm 232	8875 \pm 657	12800 \pm 641
	Soil(5.5 ns cut)	2131 \pm 233	8404 \pm 661	13135 \pm 645
105	Air	2622 \pm 239	9066 \pm 676	13788 \pm 660
	Soil(5 ns cut)	2419 \pm 233	8486 \pm 661	13355 \pm 646
155	Air	3836 \pm 302	13568 \pm 857	21197 \pm 836
	Soil (no time cut)	3865 \pm 313	13915 \pm 892	22929 \pm 869
-	Soil (sand)	623 \pm 289	5101 \pm 841	26497 \pm 820

found that extracting N and O yields from the 4.24–7.44 MeV is advantageous compared to the previous algorithm [16] because they produce 30 and 10% more counts for N and O respectively. This resulted in an estimated improvement of the statistical precision by ~ 2 and 0.5% for N and O respectively compared to the value obtained only from the 5–7 MeV portion of the spectrum.

With the present interrogation geometry, there was some background contribution to the overall time spectrum when the projectile was on the soil surface, but the background effects could be eliminated with appropriate time cuts. As an illustration, the composite time spectrum of a 60 mm (HE filled) mortar lying on soil is shown in Fig. 6 and the corresponding time correlated gamma-rays from the mortar, obtained with a 4 ns time cut is shown in Fig. 7a and b. As shown, a time window of 4 ns could effectively isolate the neutron induced gamma-rays from the mortar and reject the signals from the soil; the absence of the silicon (Si, 1.78 MeV) line from the soil is a good indicator that the cut has eliminated the soil signals. It was also noticed, that for the 155 mm

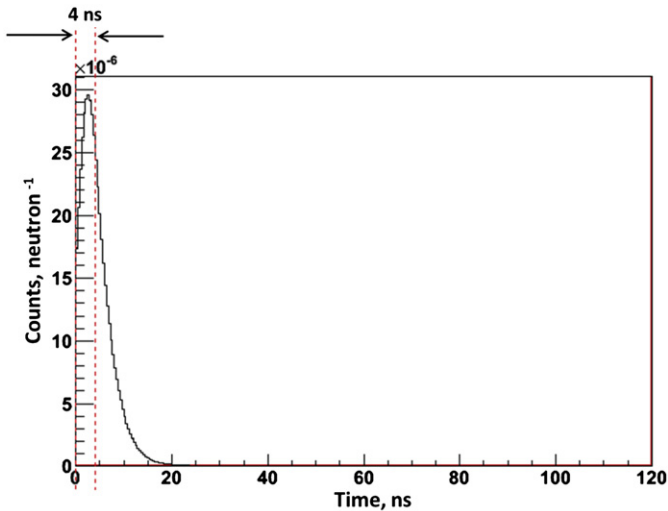


Fig. 6. Smearing time spectrum of a 60 mm mortar lying on soil. The 4 ns time cut used for eliminating soil signals and determining the time correlated gamma-rays from the UXO is shown.

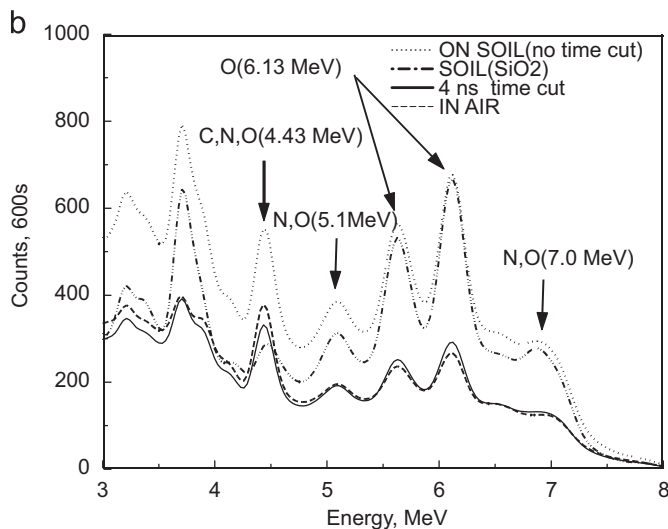
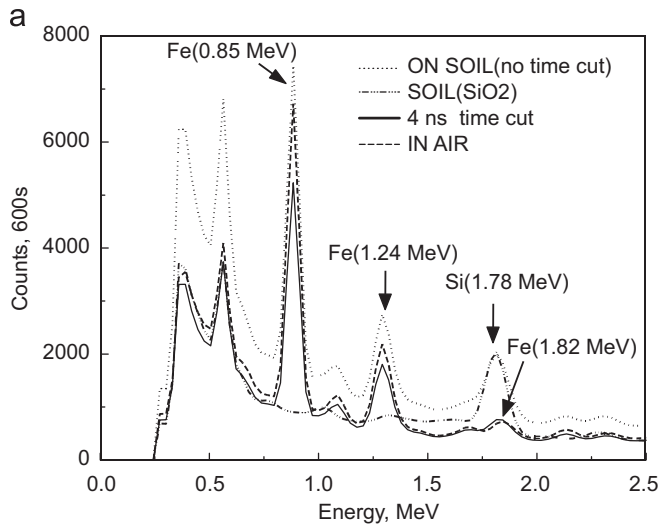


Fig. 7. (a) Gamma-ray spectra of the 60 mm mortar show that the dominant signal is from the iron (Fe) content of the shell. The 4 ns time cut shows the absence of the Si (1.78 MeV) line which is a good indicator for the successful elimination of soil signals, (b) Spectra showing the C, N and O signals.

projectile no time cuts were necessary because it completely shielded the soil.

3.3. Identification of UXO

The k_1 and k_2 values required for converting C/N and C/O counts ratios to elemental ratios, were derived for each UXO filler when situated in air. These values were then applied as a test case for predicting the elemental ratios of the UXOs situated on soil for which the soil interferences were removed by time cuts. The elemental ratios and the k_1 and k_2 values of the UXOs are shown in Table 5. A plot of the C/N and C/O counts ratios of the UXOs situated on soil (Fig. 8) shows that the algorithm can clearly discriminate an inert two-component substance like sand from the three-component HE fills. When the k_1 and k_2 conversion factors were applied to the counts ratios, all the HE fills (Composition B, TNT and Explosive D) could be further discriminated from each other (Fig. 9). In the present studies, the time-cuts were made on a visual basis by observing the disappearance of the major line due to Si at 1.78 MeV. However, complete elimination of this signal is hampered due to an unresolvable line at 1.82 MeV due to Fe. This incomplete elimination of the soil signals is reflected in a $\sim 30\%$ overestimate of the O signal at 6.13 MeV due to the O contamination of soil (see Fig. 7(a) and (b)). For field applications, the k_1 and k_2 values will be determined after time cut procedures have been standardized for complete elimination of the soil signals.

Table 5

The elemental ratios for the different high explosive fillers and the corresponding factors, k_1 and k_2 , for converting counts ratios of each UXO to elemental ratios. The UXOs were situated in air.

UXO size, mm	Explosive filler	Elemental ratio		k_1	k_2
		C/N	C/O		
57	Explosive D	1.5	0.86	4.54 ± 0.62	4.37 ± 0.49
75	TNT	2.33	1.17	7.12 ± 0.79	5.03 ± 0.49
60	Composition B	0.95	0.76	3.55 ± 0.49	4.23 ± 0.52
81	Composition B	0.95	0.76	3.65 ± 0.46	4.20 ± 0.47
105	Composition B	0.95	0.76	3.29 ± 0.39	4.00 ± 0.41
155	Composition B	0.95	0.76	3.36 ± 0.34	4.20 ± 0.37

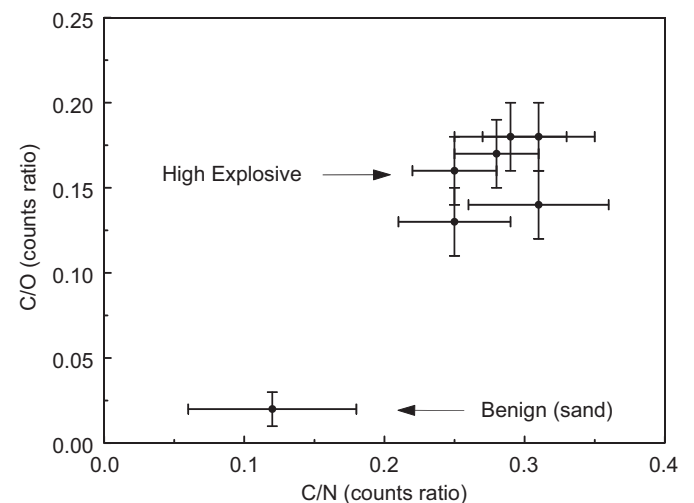


Fig. 8. The high explosive fillers of the UXOs (Composition B, TNT, Explosive D) can be differentiated from a benign substance like sand by using the C/N and C/O gamma-ray counts ratios.

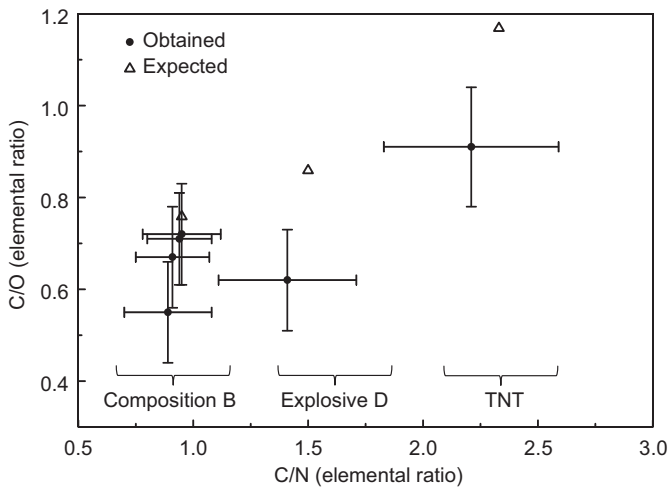


Fig.9. The high explosive fillers can be differentiated from each other on the basis of the C/N and C/O elemental ratios.

4. Conclusions

The spectral analysis method demonstrated that C, N and O signals can be extracted by a simple procedure from the 57–155 mm projectiles using an affordable and widely used low-energy-resolution detector like NaI(Tl). Further, the method has minimum computational requirements since it does not involve a library of pure elemental spectra and no spectrum fitting procedures are thus necessary to unfold the C, N and O counts from the interrogated object. The modeling data indicated that these key elements for identifying HE can be determined within a ten minute interrogation period using a timed beam of 14 MeV neutrons. Since the algorithm was developed primarily for identifying HE fillers and discriminating them from an inert substance, a three component system consisting of C, N and O has been assumed since there are no other elements present in HE that could contribute gamma-rays to the three ROIs. As a result, a two component system like sand that contains no N also produced N counts because of the N coefficient “a” operating on ROI₂. However, it was shown that it could be easily discriminated from HE simply based on its C/N and C/O counts ratio. Thus, the sensitivity of the spectral analysis scheme has the potential to differentiate the HE fillers from a benign substance like sand, at the level-one of a decision tree while at level-2, the HE explosives can be further differentiated from each other based on the C/N and C/O elemental ratios. In a field situation, time slicing procedures will be standardized for complete elimination of the soil signals for a better fit between the experimental and expected elemental ratio values. The present report illustrates the efficacy of the algorithm on synthetic spectra based on the ENDF/B-VII library of cross-sections but the utility of the scheme and the coefficients will need to be established from real spectra. While the algorithm demonstrated that it can differentiate between three types of explosive fillers that are commonly used, of which Composition B was a mixture of two different types of explosives

(RDX and TNT), it will be worthy to note that future work could include investigating the response of the algorithm to non-explosive configurations of C, N and O. More difficult scenarios using creatively made non-explosive combinations of melamine (C₃H₆N₆) and water containers would be designed in addition to investigating the spectra from commonly transported organic goods such as textiles and paper products.

Acknowledgments

This work was supported by the U.S. Department of Defense under its Strategic Environmental Research and Development Program (SERDP), Project# MR 1769. This manuscript has been co-authored by employees of Brookhaven Science Associates, LLC, under Contract no. DE-AC02-98CH10886 with the U.S. Department of Energy. The publisher, by accepting the manuscript for publication, acknowledges that the U.S. Government retains a nonexclusive, paid-up, irrevocable, worldwide license to publish or reproduce the published form of this manuscript, or allow others to do so, for U.S. Government purposes.

References

- [1] C. Bruschini, *ExploStudy*, Final Report, 2001.
- [2] C. Bruschini, *Subsurface Sensing Technologies and Applications* 2 (2001) 299.
- [3] G. Vourvopoulos, P.C. Womble, *Talanta* 54 (2001) 459.
- [4] A. Buffler, *Radiation Physics and Chemistry* 71 (2004) 853.
- [5] T. Gozani, *Nuclear Instruments and Methods*, B 213 (2004) 460.
- [6] L. Wielopolski, G. Hendrey, K.H. Johnsen, S. Mitra, S.A. Prior, H.H. Rogers, H.A. Torbert, *Soil Science Society of America Journal* Soil Science Society of America 72 (2008) 1269.
- [7] F.C. Engesser, W.E. Thompson, *Journal of Nuclear Energy* 21 (1967) 487.
- [8] R.C. Runkle, T.A. White, E.A. Miller, J.A. Caggiano, B.A. Collins, *Nuclear Instruments and Methods in Physics Research Section A* 603 (2009) 510.
- [9] A.V. Evsenin, A.V. Kuznetsov, O.I. Osetrov, D.N. Vakhtin, in: H. Schubert, A. Kuznetsov (Eds.), *Detection of Bulk Explosives*, Kluwer Academic Publishers, 2004, pp. 89–103.
- [10] G. Viesti, S. Pesente, G. Nebbia, M. Lunardon, D. Sudac, K. Nađ, S. Blagus, V. Valković, *Nuclear Instruments and Methods in Physics Research Section B* 241 (2005) 748.
- [11] S. Pesente, G. Nebbia, G. Viesti, F. Daniele, D. Fabris, M. Lunardon, S. Moretto, K. Nađ, D. Sudac, V. Valković, *Nuclear Instruments and Methods in Physics Research Section B* 261 (2007) 268.
- [12] S. Mitra, I. Dioszegi, *IEEE Nuclear Science Symposium Conference Record* (2011) Valencia, Spain.
- [13] A.V. Evsenin, et al., in: S. Apikyan, D. Diamond, R. Way (Eds.), *Prevention, Detection and Response to Nuclear and Radiological Threats*, Springer, 2008, pp. 125–140.
- [14] C. Carasco, et al., *Nuclear Instruments & Methods In Physics Research Section A* 582 (2007) 638.
- [15] W. El Kanawati, et al., *Nuclear Instruments and Methods In Physics Research Section A* 654 (2011) 621.
- [16] S. Mitra, J.E. Wolff, R. Garrett, C.W. Peters, *Physics in Medicine and Biology* 40 (1995) 1045.
- [17] D. Pelowitz (Ed.), *Los Alamos National Laboratory*, 2011, LA-CP-11-00438.
- [18] B. Perot, et al., *Applied Radiation and Isotopes* 66 (2008) 421.
- [19] B. Perot, et al., *Applied Radiation and Isotopes* (2011), <http://dx.doi.org/10.1016/j.apradiso.2011.07.005>.
- [20] C. Carasco, *Computer Physics Communications* 181 (2010) 1161.
- [21] M. Gierlik, T. Batsch, M. Moszyński, T. Szczśniak, D. Wolski, W. Klamra, B. Perot, G. Perret, *IEEE Transactions on Nuclear Science* 53 (2006) 1737.
- [22] *Global UXO/EOD Technologies Ordnance Data Sheet* (Private communication, Munitions Response, SERDP/ESTCP Support Office, HydroGeoLogic Inc., Reston, VA 20190).